Research Article

Safety Assessment of Electromagnetic Environmental Exposure for GPS Antenna of Electric Vehicle

Siyu Shang ⬤ and Mai Lu ⬤

Key Laboratory of Opto-Electronic Technology and Intelligent Control of Ministry of Education, Lanzhou Jiao Tong University, 88 West Anning Road, Anning District, Lanzhou 730070, China

Correspondence should be addressed to Mai Lu; mai.lu@hotmail.com

The present GPS (global positioning system) is widely used in electric vehicle navigation; it is usually installed in the middle-to-rear position on the car's roof, near the rear windshield. Since the GPS antenna operating frequency is 1.575 GHz, the health risk of the passengers in the car in this high-frequency electromagnetic exposure is a matter of concern. In this paper, we construct models for a GPS antenna, an electric vehicle, and a human body. Through the multiphysics field coupling calculation in COMSOL Multiphysics, a finite element simulation software, in both frequency domain and transient analysis, we obtain the electric field strength distribution, specific absorption rate, and temperature distribution of the human body at three positions inside the electric vehicle after being exposed to the GPS antenna radiation for 30 minutes. The peak human-induced electric field is 18.4 V/m, and the peak specific absorption rate is 0.193 W/kg. The 30 minute average maximum human-induced electric field is 1.6906 V/m, which is 3.1% of the ICNIRP limit, the 30 minute average whole-body SAR is 0.0036 W/kg, which is 4.5% of the ICNIRP limit, and the 30 minute average human core temperature rise is 0.06°C, which is 6% of the ICNIRP limit. In addition, we simulate the impact of three different vehicle shell materials on the level of electromagnetic exposure to the human body, which can provide reference for electromagnetic shielding design in automobiles. The results indicate that the induced electric field strength, specific absorption rate (SAR), and temperature rise in various parts of the human body did not exceed the standard limits in the latest version of ICNIRP. This suggests that the electromagnetic exposure from the GPS antenna in a typical automotive environment does not pose a threat to human health.

1. Introduction

In recent years, under the strong support and promotion of national policies, new energy electric vehicles have emerged, and antenna is an important part of the radio communication and detection system in electric vehicles. The GPS antenna used in electric vehicles emits high-frequency radiation, which has led to increasing concerns about the biological effects of exposure to high-frequency and radio-frequency electromagnetic fields in the range of 100 kHz to 300 GHz. GPS has 24 satellites, including 21 working satellites and 3 backup satellites, and theoretically GPS receivers should be able to receive signals from 4 to 11 satellites at any location on Earth at any time; therefore, the system can provide accurate and continuous three-dimensional position, velocity, and time information to users with appropriate receivers. The GPS antenna used in electric vehicles operates at a transmission frequency of 1575.42 MHz (L1 band) and 1227.6 MHz (L2 band), providing separate services for civil and military use, respectively. Circularly polarized microstrip antennas are commonly used as GPS antennas due to their lightweight, cost-effectiveness, and ability to provide omnidirectional coverage, making them popular in radar systems and mobile satellite communication as well. These antennas offer the advantage of enabling an omnidirectional orientation between the transmitter and receiver, allowing for efficient signal reception and transmission [1, 2]. In the 1970s, microstrip antennas emerged as a new antenna concept. Subsequently, microstrip antennas studied by R. E. Munson and J. Q. Howell were applied as conformal omnidirectional

antennas on rockets and missiles. With further research, microstrip antennas have been widely used in broadband radio devices ranging from 100 MHz to 100 GHz, particularly in aircraft and electric vehicles.

In electric vehicles, where passengers sit very close to the electrical system and antennas, the high currents generated in these vehicles mean that passengers may be exposed to significant electromagnetic fields [3]. In 1990, Tsukahara and Hirano used numerical analysis to calculate the electric field in the passenger compartment for vehicle surface currents and different plane wave exposures [4]. In 2003, Shiraki et al. conducted a study on the electromagnetic radiation generated by electronic devices inside a vehicle. The study employed a hybrid method combining the time-domain finite difference method and transmission line technique. This approach was utilized to determine the optimal placement of the FM radio antenna within the vehicle [5]. In 2015, Vassilev et al. measured the magnetic fields inside eight different electric vehicles (including battery, hybrid, plug-in hybrid, and fuel cell types) with different motor technologies (brush DC, permanent magnet synchronous, and induction) at frequencies of up to 10 MHz [6]. In 2019, Alessandro Arduino examined the accuracy of numerical dosimetric simulations in the context of human exposure to an electric vehicle electrostatic induction charging system. The study focuses on two optional numerical methods: the electric vector potential formulation and the electric scalar potential formulation [7]. In the same year, Gombarska et al. conducted a study using an omnidirectional 8 dBi antenna to measure the electric field intensity generated by in-vehicle communication devices and high-frequency electronic devices within the 500 MHz–3300 MHz frequency range. The study demonstrated that the exposure to the electromagnetic environment in electric vehicles did not exceed the established safe range [8]. In addition, Shah and Yoo et al. conducted measurements to assess the exposure of manikins with implanted pacemakers to electromagnetic fields emitted by electric vehicle wireless power transmission systems. The study revealed that passengers with neuro-stimulation implants and implanted hip joints with prostheses experienced specific absorption rate (SAR) values exceeding the established safety standard by more than 10 g of human tissue [9]. In 2021, WenTing and Mai conducted an evaluation of the safety of electromagnetic exposure to the human central nervous system from an electric vehicle magnetically coupled resonance wireless charging system. The study demonstrated that the maximum magnetic induction and electric field strengths in the human head were measured as $0.9\,\mu$T and 0.18 V/m, respectively. These values were found to be below the public exposure limits set by the International Commission on Non-Ionizing Radiation Protection, which are $27\,\mu$T for magnetic induction and 2.97 V/m for electric field strength [10]. In the same year, De Santis et al. conducted an evaluation of external magnetic fields emitted by wireless power transfer (WPT) systems and internal electric fields generated by human models during the charging process of small electric vehicles (EVs). The study revealed that the obtained results exceeded the reference levels set by the International Commission on Non-Ionizing Radiation Protection (ICNIRP) in the driving position [11].

The effects of high-frequency electromagnetic fields generated by antennas on human health have been studied for decades. In 1993, Dimbylow conducted a study where they used the finite difference in time domain (FDTD) method to calculate the radiation emitted by a dipole antenna on a realistic head model. Their analysis led to the conclusion that highly conductive tissues have a greater tendency to absorb the energy preferentially [12]. In 2008, Yu et al. simulated the electromagnetic characteristics of a whip antenna of a car at different positions based on the CST FIT technique [13]. In 2009, Hirata and Ida conducted a simulation study where they exposed a vehicle to a high-frequency electromagnetic environment, including radar and antennas. Their findings revealed that the presence of the human body model led to the suppression of standing waves near the vehicle's dashboard. This suppression was attributed to the power absorption of the human body, particularly in the frequency range of 100–200 MHz [14]. Wessapan et al. investigated the specific absorption rate (SAR) distribution and temperature field distribution of a real human body model subjected to electromagnetic radiation from antennas operating at 900 MHz and 1800 MHz, respectively, as influenced by the operating frequency and the size of the distance between the antenna and the human head [15]. In 2021, Kumar and Imaculate presented a hybrid half-mode substrate integrated waveguide (HMSIW) diplex antenna for on-body transceiver application with two resonant frequencies of 4 GHz and 4.79 GHz. This literature has simulated the radiation from the antenna to the human head and body and verified the specific absorption rate. Due to the unidirectional nature of the radiation from this antenna, the SAR values are low [16].

At present, investigations have revealed that the research on the impact of high-frequency environments in electric vehicles on the human body is still not very comprehensive, particularly in the context of the effects of onboard antennas on human subjects. And in this paper, multiphysics field coupling calculations are performed. A comprehensive assessment of the safety of human electromagnetic exposure has been carried out in COMSOL software. We simulated not only the EM-induced E-field distribution and SAR distribution of the human body but also the whole-body average induced E-field, SAR, and head temperature field distributions after 30 minutes of EM irradiation environment, and then compared the results with the latest international standard ICNIRP (2020). In addition, I believe that the research methodology used in this study can significantly reduce the computational effort of similar research endeavours, providing a more economical and efficient approach.

2. Model Building and Calculation Method

2.1. GPS Antenna Model

2.1.1. GPS Antenna Design Principle. In this paper, we present the design of a right-handed circularly polarized GPS receiving antenna. The antenna is fed by a coaxial probe, with a center frequency of 1.575 GHz. To achieve

circular polarization, an angle cut is employed, ensuring that the antenna radiates circularly polarized waves. The axis ratio of the circularly polarized wave at the center frequency is maintained at less than 2.0 dB. The excitation source of the model is a voltage source, the excitation source is a sinusoidal voltage signal excitation, the amplitude is set to 1 V, the impedance is 50 Ω, the input power is 20 mw, and the excitation source is set at the base of the antenna [17]. There are two ways to feed the rectangular microstrip antenna to obtain circular polarization characteristics, one is single point feed and the other is orthogonal double feed. The GPS antenna model used in this paper is a single-point fed tangential circularly polarized microstrip patch antenna. By a special feeding method, the circularly polarized rectangular patch microstrip antenna can be obtained. The key to circular polarization is to excite a line polarization wave with two polarization directions of equal orthogonal amplitude and 90° phase difference. According to the cavity mode theory, a single rectangular microstrip antenna fed by a point can produce two simple parallel modes with equal polarization orthogonal amplitude but cannot form a 90° phase difference. In order to form a 90° phase difference between the simple and parallel modes, a simple and parallel mode separation unit is introduced in the regular shape of the single microstrip antenna, the most common form of separation unit is to cut the corner on the two diagonals of the rectangular patch, so that the resonant frequency of the simple and orthogonal modes are separated, and the operating frequency is chosen between the two frequencies. When the size of the simple parallel mode separation unit is appropriately selected, it results in the formation of circular polarization radiation. Specifically, at the operating frequency, the equivalent impedance of one mode exhibits a phase angle leading by 45%, while the equivalent impedance of another mode lags by 45%. This phase difference between the modes facilitates the generation of circularly polarized radiation [18].

2.1.2. GPS Antenna Design Steps. Coaxial line feed, also referred to as backfeed, involves a coaxial socket mounted on a grounding plate. The conductor within the coaxial line is connected to the radiation patch through the dielectric substrate. By identifying the correct location for the feed point, a favorable match can be achieved. In order to design a right circularly polarized microstrip antenna, it is necessary to relocate the coaxial line feed point to the position depicted in Figure 1. In addition, two appropriately sized isosceles triangles need to be cut out at the opposite corners of the square metal patch.

Based on the dielectric substrate parameters, we can employ calculations from formulas (1) to (6) to determine the resonant frequency of 1.575 GHz for the initial size of the radiation patch. By adjusting the width W and length L of the radiation patch, as well as the side length of the square dielectric substrate (*Length*), we can set the distance d_p and the tangent triangle waist length a from the center of the fine-tuned feed point to generate circularly polarized waves [19]. The position of the coaxial feed point with an input
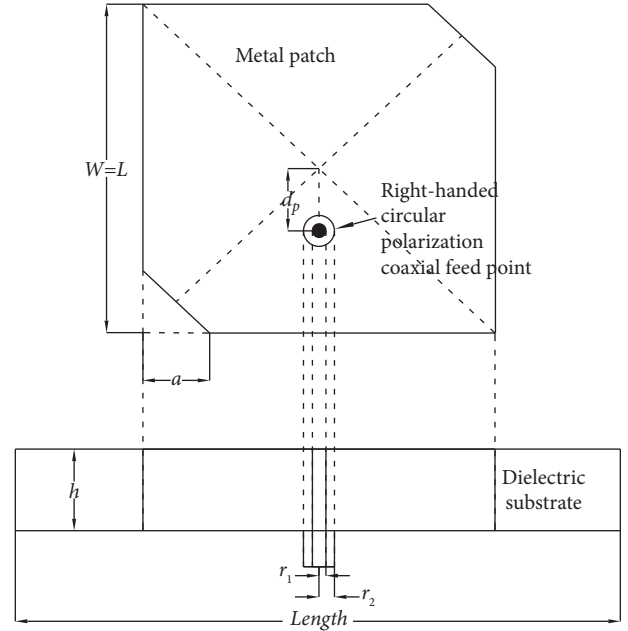

Figure 1: GPS single point fed circularly polarized microstrip antenna structure.

impedance of 50 Ω is estimated based on the dielectric substrate parameters and the initial size of the radiating patch. The actual size of the radiating patch and the precise position of the 50 Ω feed point at the resonant frequency of 1.575 GHz are determined through parametric scan analysis. The optimization objective is to achieve a return loss of less than −20 dB, an axial ratio of less than 3 dB, and a radiation patch size and feed point position that meet the design requirements.

For the rectangular microstrip antenna operating at frequency f, the width w of the high-efficiency radiation patch can be designed using the following equation:

$$w = \frac{c}{2f}\left(\frac{\varepsilon_r + 1}{2}\right)^{-(1/2)}, \tag{1}$$

where c is the speed of light and ε_r is the permittivity of the dielectric substrate.

The length of the radiation patch is taken as $\lambda_e/2$, where λ_e is the wavelength of the guided wave within the medium:

$$\lambda_e = \frac{c}{f\sqrt{\varepsilon_e}}. \tag{2}$$

Due to the consideration of the edge-shortening effect, the actual radiation cell length L should be

$$L = \frac{c}{2f\sqrt{\varepsilon_e}} - 2\Delta L, \tag{3}$$

where ε_e is the effective dielectric constant and ΔL is the equivalent radiation gap length. They can be calculated separately by the following equation, i.e.:

$$\varepsilon_e = \frac{\varepsilon_r + 1}{2} + \frac{\varepsilon_r - 1}{2}\left(1 + 12\frac{h}{w}\right)^{-(1/2)}. \tag{4}$$

The following equation can also be used to directly approximate the location of the feed point when the input impedance is 50 Ω.

$$L_1 = \frac{L}{2}\left(1 - \frac{1}{\sqrt{\xi_{re}}}\right),$$
$$\Delta L = 0.412h\frac{(\varepsilon_e + 0.3)(w/h + 0.264)}{(\varepsilon_e - 0.258)(w/h + 0.8)}, \tag{5}$$

where

$$\xi_{re}(L) = \frac{\varepsilon_r + 1}{2} + \frac{\varepsilon_r - 1}{2}\left(1 + 12\frac{\hbar}{L}\right)^{-(1/2)}. \tag{6}$$

First, the size of the patch is estimated using equation (2). The antenna structure consists of the patch, dielectric substrate, and ground plane, with their material parameters shown in Table 1. The patch, ground plane, inner conductor, and outer conductor of the coaxial cable are assumed to be ideal conductors. An air domain in the shape of a sphere is set outside the antenna and truncated by a perfectly matched layer (PML) to absorb all radiation. To analyze the electromagnetic waves more accurately, all domains are divided into grids, with the maximum grid size not exceeding one-fifth of the wavelength. The antenna is excited by a coaxial collector port with an input voltage of 1 V and a relative dielectric constant of 1. The port is located on the bottom surface of the coaxial-fed outer cylindrical structure. Due to the high input impedance at the edge of the patch and low input impedance at the center, the position of the coaxial feed cable needs to be adjusted to match the 50 Ω reference impedance. In addition, to find the resonance point at 1.575 GHz, a parameterized scan of the chamfer size of the patch is performed. The main process of the parameter scan is shown in Table 2.

Finally, the design results are given, as shown in Table 3. In practice, the shell of the antenna is mostly of shark fin shape. The material is carbon fiber, because it has very little effect on the antenna radiation characteristics, so in order to simplify the calculation, the antenna shell is designed into a square model with side length of 120 mm, as shown in Figure 2.

2.2. Model of Human Body.
Based on the internationally common proportions of the human body, a sitting model of an adult with a height of 1.75 meters has been established. The height of the sitting model is 1300 mm, and the shoulder width is 520 mm. The parameters of the simple three-layer head model are: scalp radius is 92 mm, skull radius is 85 mm, and cerebrum radius is 80 mm. As early as 1968, Rush and Driscoll proposed a three-sphere model to replace the real human head model for numerical calculations [20]. They used three concentric spheres with different resistivities to represent the cerebrum, skull, and scalp. The geometry and coordinate system of the three-sphere mathematical model and the nature of its fit to the head were derived from the standard methods of field theory and the potential energy equation (21). The validity of the model was tested by means of an electrolytic bath containing a human skull and compared with in vivo data from the inside of a monkey's brain and from the surface of the human head, and can be used to calculate equivalently the dielectric parameters of the human head.

The sitting manikin is shown in Figure 3. The dielectric constants and conductivities of human tissues at the corresponding operating frequencies are obtained according to the fourth order Cole-Cole model, where the average values of cerebral white matter, cerebral gray matter, and cerebrospinal fluid are used for the brain, and the average values of four tissues, skin, blood, muscle and bone are taken for the trunk tissues.

2.3. Complete Vehicle Model.
Construct a simplified model of a car body based on the design of the Chinese standard car model. The electric car body model, as depicted in Figure 4, primarily utilizes aluminum alloy and glass materials. The dimensions of the body are 4600 mm × 1800 mm × 1500 mm. A three-dimensional Cartesian coordinate system is established, and the left rear endpoint of the electric car was set as the coordinate origin. The positions of the mannequin and the onboard GPS antenna are listed in Table 4.

3. Principles and Methods of Human Electromagnetic Exposure Assessment

3.1. Calculation Method for Electromagnetic Exposure Assessment.
When using the RF Module in COMSOL software for simulation, the main electromagnetic wave equations involved are shown in Table 5.

Φ denotes the magnetic flux through the closed equivalent surface of C and Js denotes the surface current density. Deriving the boundary conditions corresponding to the surface integrals in Maxwell-Ampere's and Faraday's laws is a process of taking the limit, which requires obtaining the flux perpendicular to the limiting surface. For a surface that tends to be infinitesimal to vanishing, the contribution of this process is zero, so that at rest, the boundary conditions corresponding to Maxwell-Ampere's and Faraday's laws are the same.

By combining Maxwell-Ampere's law and Faraday's law, a second-order fluctuation equation can be obtained by substituting the rotations of one of the equations into the other, and the system of equations resulting from the union of these two first-order equations represents an electromagnetic wave. Since the conductivity of the antenna material is set to 0, the plane wave equation is

$$k \times (k \times E) + \omega^2 \mu\varepsilon E = 0. \tag{7}$$

The far field of an antenna can be calculated from the near field using the Stratton-Chu formula. In 3D space, the formula is as follows:

$$E_P = \frac{jk}{4\pi}r_0 \times \int_S [n \times E - \eta r_0 \times (n \times H)]\exp(jkr \cdot r_0)dS. \tag{8}$$

Thus, the relative far-field radiation pattern is given by plotting $|E_P|^2$. The use of a Perfectly Matched Layer (PML) enables the absorption of outgoing radiation over a wide range of frequencies and angles of incidence to improve simulation accuracy.

TABLE 1: Material parameters of the antenna.

Name	Relative permittivity	Relative permeability	Electrical conductivity (S/m)
Patch	3.38	1	0
Outer conductor of the coaxial cable	2.1	1	0
Dielectric substrate	3.38	1	0

TABLE 2: Variation of the antenna radiation parameters (output) for different inputs.

Input parameters				Output results	
h	L	d_p	a	S_{11} return loss (dB)	Resonate peak (GHz)
1.5240	50.26	10.000	3.5	−17.35	1.574
1.5240	50.25	10.000	3.5	−18.70	1.574
1.6510	50.25	10.000	3.9	−18.70	1.575
1.5360	50.25	10.830	3.9	−19.95	1.576
1.5354	50.25	10.815	3.9	−20.10	1.575
1.5354	50.25	10.850	3.9	−18.60	1.575
1.5354	50.25	10.810	3.9	−18.30	1.575

TABLE 3: GPS antenna model parameters.

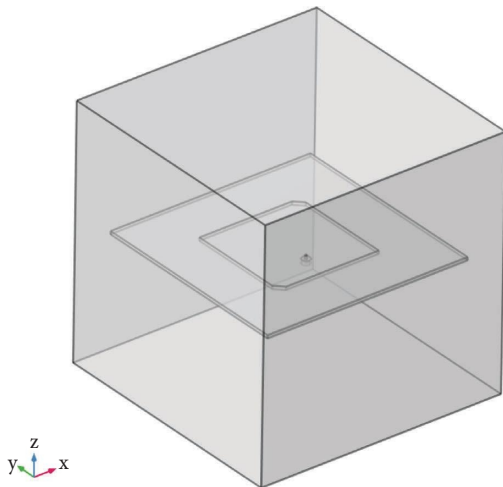| Parameter	Value (mm)
h	1.5354
L	50.25
W	50.25
Length	50.00
d_p	10.815
a	3.9
r_1	0.6
r_2	1.5

FIGURE 2: GPS antenna and outer shell model.

A major focus of bioelectromagnetic exposure assessment is the dielectric properties of living organisms, as different dispersion phenomena occur in the same biological tissue at different frequency bands, resulting in changes in the relative permittivity and conductivity of biological tissues with frequency [22]. In 1996, Gabriel et al. derived the
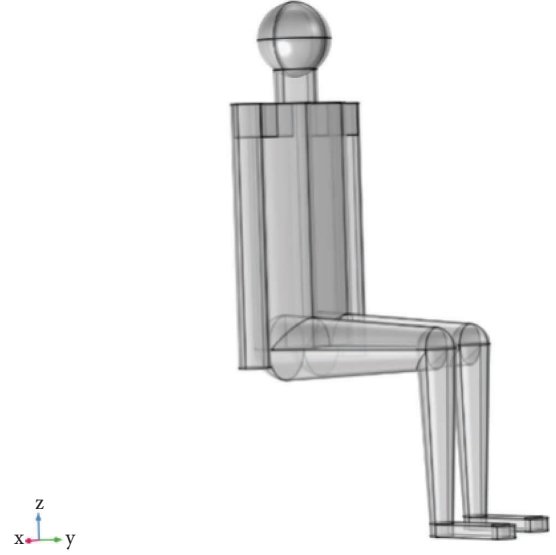

FIGURE 3: Human sitting posture model.

fourth-order Cole-Cole model based on the results of RHCole and KSCole studies, which can be applied to calculate the dielectric constant of biological tissues in the frequency band of 10 Hz-20 GHz [23]. The fourth-order Cole-Cole model is shown in the following equation:

$$\widehat{\varepsilon}_r = \varepsilon_r' - j\varepsilon_r'' = \varepsilon_{r\infty} + \sum_{n=0}^{4} \frac{\Delta\varepsilon_n}{1 + \left(j\omega\tau_n\right)^{1-\alpha}} + \frac{\sigma_i}{j\omega\varepsilon_0}, \tag{9}$$

where $\widehat{\varepsilon}_r$ is the complex relative permittivity, ε' is the real part of the complex relative permittivity, also known as the relative permittivity, ε_r'' is the imaginary part of the complex relative permittivity, also known as the loss factor, $\varepsilon_{r\infty}$ is the value of the relative permittivity at the optical frequency, ω is the angular frequency in rad/s, which can be found from the frequency, and $\varepsilon_0 = 8.854187817 \times 10^{-12}$ is the permittivity in vacuum in F/m. $\Delta\varepsilon_n$ is the increment of dielectric constant, τ_n is the central relaxation time, α is the relaxation distribution time, which usually takes the value between 0 and 1, and σ_i is the conductivity of ions. In this paper, the conductivity of similar tissues is used to simulate various tissues in the head model based on the GPS antenna frequency of 1.575 GHz [24], and the calculated dielectric parameters and the electromagnetic power loss density (emw) heat sources of the three-layer spherical head model and the human trunk are shown in Table 6.

The effect of electromagnetic exposure on the human body in the 1.575 GHz band is dominated by the heating effect on the human body, a physical process expressed in biometrics as SAR. SAR is the electromagnetic power
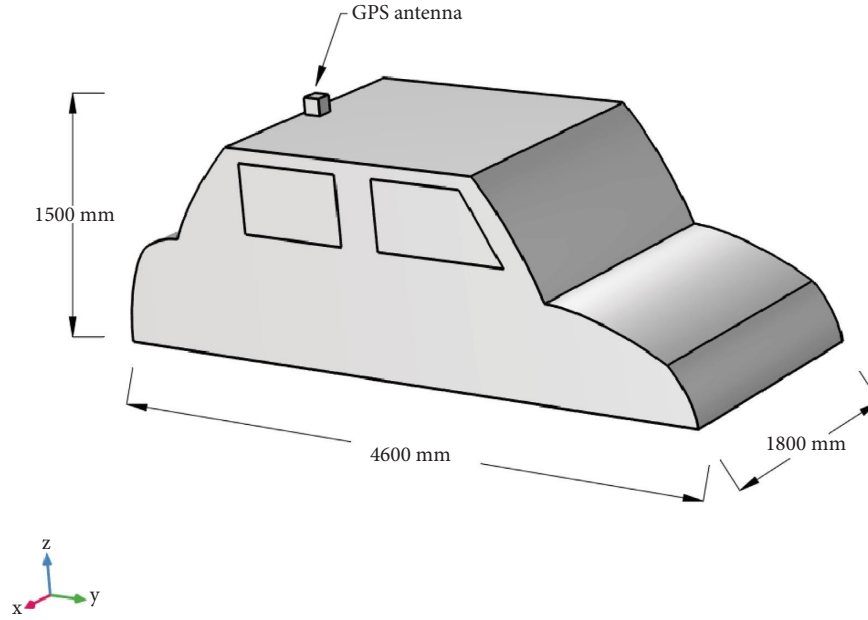
FIGURE 4: Simple model of electric vehicle.

absorbed per unit time mass of human tissue, and the energy increment dW is absorbed in the time derivative of the mass increment dm for a given density ρ and volume dV [25]. The mathematical expression of SAR is

$$\text{SAR} = \frac{d}{dt}\left(\frac{\text{dW}}{\text{dm}}\right) = \frac{d}{dt}\left(\frac{\text{dW}}{\rho\text{dV}}\right). \quad (10)$$

The basic SAR-based equation:

$$\text{SAR} = \frac{\sigma}{\rho}E^2 = c\frac{\Delta T}{\Delta t}, \quad (11)$$

where SAR is the specific absorption rate (W/kg), σ is the electrical conductivity (S/m), ρ is the tissue density (kg/m^3), E is the electric field strength (V/m), and c is the specific heat capacity.

Human head tissue absorbs electromagnetic radiation and converts it into joule heat [26]. In this paper, the transient bioheat equation by Pennes [27] is employed in the COMSOL simulation software to describe a series of heat transfer processes occurring when electromagnetic radiation penetrates through the scalp layer and reaches the skull and cerebrum layers. This allows for the analysis of temperature distribution in various tissue layers of the human head model. The heat transfer equation is expressed by the following formula:

$$\rho C\frac{\partial T}{\partial t} = \nabla \cdot (k\nabla T) + \rho_b C_b \omega_b (T_b - T) + Q_{\text{met}} + Q_{\text{ext}}, \quad (12)$$

where ρ is the tissue density (kg/m^3); C is the tissue-specific heat capacity (J/(kg·°C)); k is the thermal conductivity (W/(m·°C)); T is the tissue temperature (°C); T_b is the blood temperature (°C); ρ_b is the blood density (kg/m^3); C_b is the blood-specific heat capacity (J/(kg·°C)); ω_b is the blood irrigation rate (s^{-1}); Q_{met} is the metabolic heat source (W/m^3); and Q_{ext} is the external heat source (W/m^3).

The heat transfer between the tissue and the blood stream is approximated by $\rho_b C_b \omega_b (T_b - T)$. The external heat source is the heat loss from the absorption of electromagnetic irradiation by the biological tissue. It can be defined as shown in the following equation:.

$$Q_{\text{ext}} = \frac{1}{2}\sigma_{\text{tissue}}|E|^2 = \rho \cdot \text{SAR}, \quad (13)$$

where $\sigma_{\text{tissue}} = 2\pi f \varepsilon_r' \varepsilon_0$; ε_r' is the relative permittivity of the tissue; and ε_0 is the (absolute) permittivity in vacuum.

3.2. Electromagnetic Exposure Safety Assessment Criteria. In order to unify the level of protection related to electromagnetic exposure, the World Health Organization (WHO) has recommended the International Commission on Non-Ionizing Radiation Protection (ICNIRP) guidelines and the Institute of Electrical and Electronics Engineers (IEEE) C95.1-2005 as the safety assessment standards for electromagnetic exposure to all countries around the world. In March 2020, ICNIRP published the latest edition of the ICNIRP Guidelines for human protection against exposure to radiofrequency electromagnetic fields (emf) in the range of 100 kHz–300 GHz (referred to as "RF"). According to the latest ICNIRP guidelines (2020), for frequencies ranging from 30 MHz to 2 GHz, in the far-field region, compliance is demonstrated if the incident power density, incident electric field strength, or incident magnetic field strength (only one of them is required) does not exceed the reference levels. The safety limits for public human-induced electric field exposure in electromagnetic fields from 100 kHz to 300 GHz for an average of 30 minutes are shown in Table 7, and the reference levels for whole-body exposures for an average of 30 minutes are shown in Table 8 [28]. Whole-body average SAR values are to be averaged over the entire body and over a 30 minute period. The 30 minute averaging time is

TABLE 4: Position of the human model and GPS antenna in the vehicle.

Coordinates (mm)	Rear middle seat position	Rear window seat position	Driver's seat position	GPS antenna position
Head x-axis coordinates	900	350	350	900
Head y-axis coordinates	1220	1220	2670	1090
Head z-axis coordinates	1352	1352	1352	208
Distance from the top of the head to the antenna feed port	247	602	1685	Not applicable

TABLE 5: Electromagnetic wave equations.

Name	Differential form	Integral form	Boundary conditions
Gauss's law for magnetism	$\nabla \cdot B = 0$	$\oint_S B \cdot \mathrm{nds} = 0$	$n \cdot (B_2 - B_1) = 0$
Maxwell-Ampere's law (static magnetism)	$\nabla \times H = J + (\partial D/\partial t)$	$\oint_C H \cdot \mathrm{dl} = \mathrm{I} + \oint_S (\partial D/\partial t) \cdot \mathrm{ds}$	$n \times (H_2 - H_1) = J_S$
Faraday's law	$\nabla \times E = -(\partial B/\partial t)$	$\oint_C E \cdot \mathrm{dl} = -\oint_S (\partial B/\partial t) \cdot \mathrm{ds} = -(\partial \Phi/\partial t)$	$n \times (E_2 - E_1) = 0$

TABLE 6: Dielectric and heat source parameters of human tissues at 1.575 GHz.

Human model tissues	Relative permittivity	Electrical conductivity (S·m^{-1})	Electromagnetic power loss density (emw) heat source (W·m^{-3})
Scalp	39.28	1.10	12.693
Skull	12.33	0.27	2.6968
Cerebrum	51.82	1.62	3.8098
Trunk	41.31	1.12	Not

TABLE 7: Reference levels for exposure, averaged over 30 minutes and the whole body, to electromagnetic fields from 100 kHz to 300 GHz (unperturbed rms values).

Exposure scenario	Frequency range	Incident E-field strength; einc (V/m)
General public	0.1–30 MHz	$300 f_M^{0.7}$
	>30–400 MHz	27.7
	>400–2000 MHz	$1.375 f_M^{0.5}$
	>2–300 GHz	Not applicable

TABLE 8: Basic restrictions for electromagnetic field exposure from 100 kHz to 300 GHz, for averaging intervals ≥6 min.

Exposure scenario	Frequency range	Whole-body average SAR (W/kg)
General public	100 kHz–6 GHz	0.08
	>6–300 GHz	0.08

intended to take into account the time required to reach a steady-state temperature, while requiring that the whole-body human body warming value does not exceed 1°C.

The frequency of the GPS antenna is 1.575 GHz. Corresponding to the data in the table, the safety limit of the human body–induced electric field at this frequency is 54.57 V/m, and the safety limit of the whole body average SAR is 0.08 W/kg.

3.3. Computational Validation. In order to test the accuracy of the research modelling and methodology, this paper is compared with the findings in the literature [29]. In the literature, there are studies that focus on the use of UHF Radio Frequency Identification (UHF RFID) passive tagged fixed multiantenna readers for performing SAR assessments in the human body. As depicted in Figure 5, the dimensions of the antenna patch are 122.5 mm in width and 99.6 mm in length. The substrate measures 138.3 mm in width and 131.5 mm in length, with a thickness of 1.52 mm. The copper patch utilized for the antenna possesses a conductivity of 5.813×10^7 S/m, and a relative dielectric constant of 1. The substrate material employed is RO3003, which has a conductivity of 2.2×10^{-4} S/m. The ground surface is set as PEC (perfect electrical
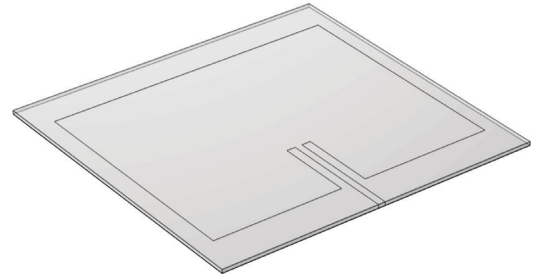

FIGURE 5: Structure of a fixed I-RFID reader microstrip patch antenna.

conductor). The UHF RFID antennas were located at a distance of 5 cm to the closest surface of the human body. In the exposed scenario, there are three antennas. The center height of the lower antenna is 626 mm, that of the middle antenna is 1018 mm, and that of the upper antenna is 1410 mm, as shown in Figure 6. In this paper, the corresponding microstrip patch antenna is modelled using COMSOL simulation software, the input power of the excitation source is 1 W, and the operating frequency is 866 MHz. The electrical parameters of the organisation in the human body model at 866 MHz are calculated from the fourth order Cole-Cole model, as shown in Table 9.

After performing numerical analysis using the COMSOL software, the human body's 30 minute whole-body average specific absorption rate (SAR) value was calculated. The distribution of these simulated values is depicted in Figure 7. In order to assess the accuracy of the simulation, the obtained SAR values were compared with the corresponding values reported in the literature. The results of this comparison are presented in Table 10.

The simulation results show that the 30 minute whole-body average SAR value of the human body is 0.0118 W/kg, compared with the results obtained from the simulation in the literature of the 30 minute whole-body average SAR value of 0.012 W/kg. The error ratio of 1.67%, which is within the permissible range of error, due to the different selection of the mesh sectioning fineness of the COMSOL software as well as the computational differences between different software, will inevitably result in the existence of errors. The validation is primarily aimed at confirming the accuracy of
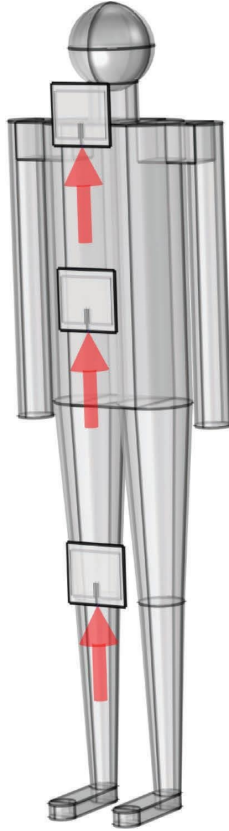
Figure 6: Antenna position diagram of human body.

Figure 7: Exposure scenarios to EMF near UHFI-RFID multi-antenna readers.

Table 9: Permittivity and conductivity of human tissues at 866 MHz.

Human model tissues	Relative permittivity	Electrical conductivity (S·m^{-1})
Scalp	41.58	0.86
Skull	12.95	0.17
Cerebrum	53.53	1.30
Trunk	41.78	0.87

Table 10: Comparison of SAR results and error analysis.

Value	30 minute whole-body average SAR (W/kg)
Simulated value	0.0118
Literature value	0.0120
Error value	1.67%

the theories, methods, and COMSOL software employed in this study. This paper constructed a microstrip patch antenna model of the same type as described in the literature. The model was utilized to simulate the electromagnetic field distribution when a human body is exposed to the electromagnetic environment of the antenna. A comparison of the results revealed errors of less than 5%, indicating that the methods and software utilized in this study are suitable for electromagnetic simulation calculations involving human subjects.

4. Safety Assessment of Human Electromagnetic Exposure in Electric Vehicles under GPS Antenna Operating Conditions

4.1. GPS Antenna Radiation Characteristics Simulation. For high-frequency electromagnetic fields, the characterization of the system requires defining scattering parameters (S-parameters) based on the electric field. To achieve this, an eigenmode expansion of the electromagnetic fields on the ports is necessary. This expansion allows for the conversion of an electric field pattern on a port into a scalar complex number representing the voltage in transmission line theory. Assume that an eigenmode analysis has been performed on the ports 1, 2, 3, . . ., and that the electric field patterns E1, E2, E3, . . ., of the fundamental modes on these ports are known. Further, assume that the fields are normalized with respect to the integral of the power flow across each port cross section, respectively. The port excitation is applied using the fundamental eigenmode, the mode with subscript 1. The computed electric field E_c on the port consists of the excitation plus the reflected field. That is, on the port boundary where there is an incident wave, the computed field can be expanded in terms of the mode fields as

$$E_c = E_1 + \sum_{i=1} S_{i1} E_i, \tag{14}$$

where as on all other port boundaries, the computed field is given by

$$E_c = \sum_{i=1} S_{i1} E_i. \tag{15}$$

The S-parameter for the mode with index k is given by multiplying with the conjugate of the mode field for mode k and integrating over the port boundary. Since the mode fields for the different modes are orthogonal, the following relations are obtained for the S-parameters.

$$S_{11} = \frac{\int_{\text{port1}} \left((E_c - E_1) \cdot E_1^* \right) dA_1}{\int_{\text{port1}} \left(E_1 \cdot E_1^* \right) dA_1}, \tag{16}$$

$$S_{21} = \frac{\int_{\text{port2}} \left(E_c \cdot E_2^* \right) dA_2}{\int_{\text{port2}} \left(E_2 \cdot E_2^* \right) dA_2}, \tag{17}$$

$$S_{31} = \frac{\int_{\text{port3}} \left(E_c \cdot E_3^* \right) dA_3}{\int_{\text{port3}} \left(E_3 \cdot E_3^* \right) dA_3}. \tag{18}$$

To get S22 and S12, excite port number 2 in the same way.

In this paper, the radiation performance of the antenna is simulated in COMSOL software, and the electromagnetic wave reflection capability is analyzed. As Figure 8 gives the GPS antenna ideal case S_{11} parameter curve, the horizontal coordinate is frequency, the vertical coordinate is return loss, its resonance point is located at 1.575 GHz, and the return loss at this point is -20 dB. Therefore, the antenna exhibits good return loss. Figure 9 shows the polar plot of antenna axis ratio, all of which are in line with the design principle of GPS antenna. Figure 10 shows the antenna surface electric field distribution; the maximum electric field is 3110 V/m. The four corners of the patch exhibit high electric field, which is consistent with the characteristics of circularly polarized antennas. Figure 11 shows the antenna three-dimensional far field gain; the maximum gain is 6.83 dBi. Figure 12 represents the antenna voltage standing wave ratio (VSWR), and the VSWR values near the resonance points are all below 2, indicating that the antenna has good input matching. The characteristics of the GPS antenna in this work are compared with other literature, as shown in Table 11.

4.2. Electric Field Intensity Distribution in Space of Electric Vehicles.
Figure 13 shows the three-dimensional distribution of the induced electric field intensity in the electric car body, wherein the radiation energy it receives is more uniformly spread throughout the car, which is due to the omnidirectional nature of the radiation of the circularly polarized antenna. The maximum value of the induced electric field on the car body is 61.9 V/m, which is located on the rear window glass of the car.

4.3. Human Electric Field Intensity Distribution.
Figures 14–16 show the induced electric field intensity distributions of the whole human body and head at the middle rear seat position, the rear window seat position, and
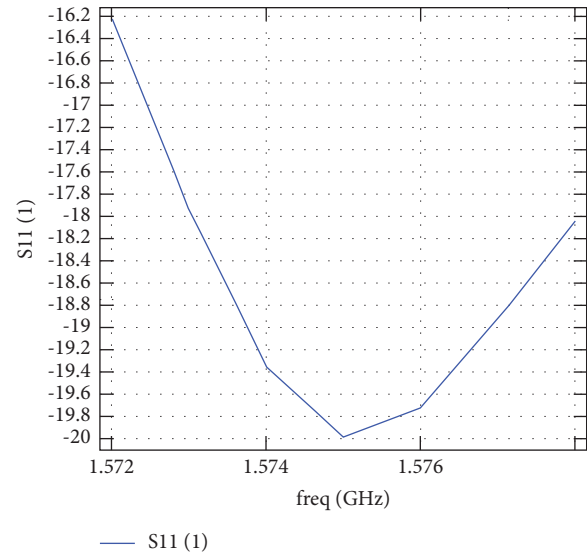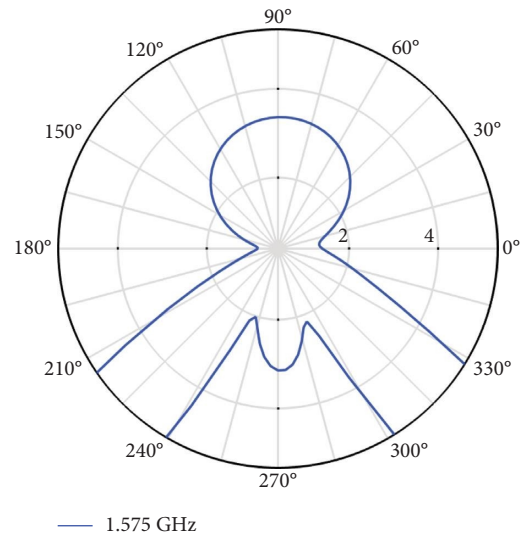

FIGURE 8: Antenna S11 parameter.

FIGURE 9: Antenna axis ratio polar plot.

the driver's seat position, respectively, as well as the XY and YZ plane slices of the head. Table 12 gives the details of the maximum values and distributions of the induced electric field intensity of the human body model and the ball head model under the operating frequency of 1.575 GHz of the GPS antenna, respectively.

As can be seen from Figures 14–16, the distribution of electric field intensity in the whole human body has no obvious rule, which shows that the direction of the electric field generated by the GPS antenna is scattered and not concentrated, and the maximum value does not exceed the ICNIRP guideline of the public exposure safety limit of 54.57 V/m. From the head slices, it can be seen that the electric field gradually decreases from outside to inside the head, and all of them are within the safety standard.
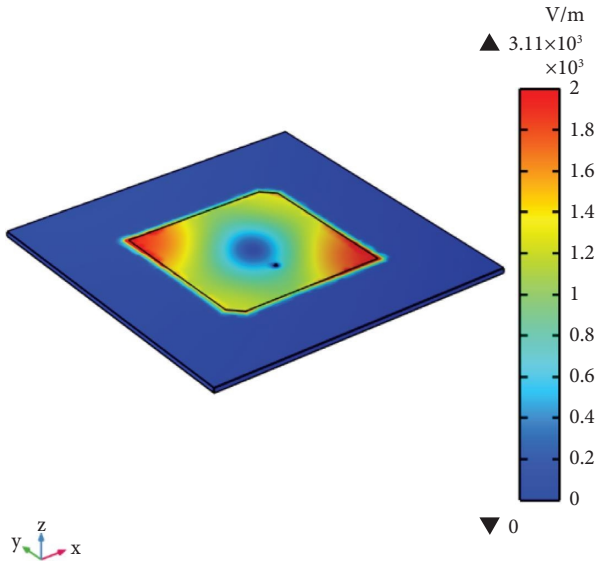
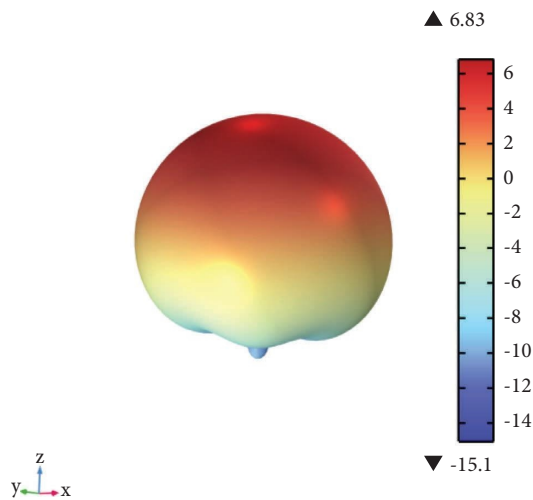Figure 10: Antenna electric field intensity distribution.

Figure 11: Antenna three-dimensional far-field gain.

Figure 12: Antenna voltage standing wave ratio (VSWR).

4.4. Human SAR Distribution. For high-frequency electromagnetic radiation, the applied electric field will produce an induced electric field in the human body, and human tissues are lossy media, so there will be a current generated by the electric field, absorbing and dissipating electromagnetic energy, thus the electric field causes a heating effect on human tissues. According to the safety guidelines of ICNIRP, the exposure threshold for the general public is generally 0.08 W/kg, which has been widely used in recent years in bioelectromagnetic exposure studies. Figures 17–19 show the distribution of the specific absorption rate of the antenna on the human body in the middle rear seat position, the rear window seat position, and the driver seat position, respectively.

The SAR values of the human head model and the three-layer spherical head model consisting of the scalp layer, the skull layer, and the cerebrum layer at the operating frequency of 1.575 GHz of the GPS antenna are given in detail
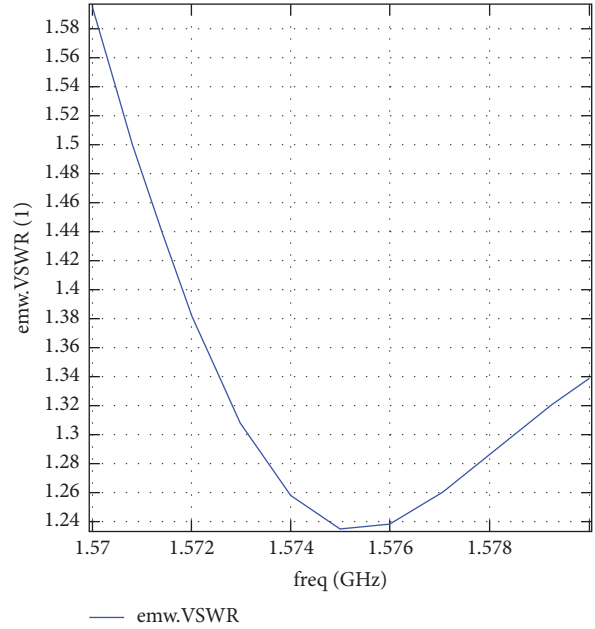
in Table 13. Comparing with Table 13, it can be seen that as the electromagnetic wave generated by the antenna penetrates the human head model, the SAR value is highest in the scalp layer of the human head model, decreases after passing through the skull layer, and is lowest after entering the cerebrum layer. This is determined by the electrical characteristics of the skull layer, where a large amount of electromagnetic waves are absorbed by the skull layer, thus reducing the number of electromagnetic waves entering the cerebrum layer.

4.5. Whole-Body Average of 30 Minute Exposure to GPS Antenna Electromagnetic Fields. The electromagnetic waves generated by the vehicle GPS antenna penetrate the human body. Due to the electromagnetic coupling effect and the cumulative effect of radiation over time, each tissue layer of the human body absorbs the electromagnetic radiation energy and converts it into heat loss. The space averaged induced electric field strength values, whole body averaged SAR, temperature rise values, and ICNIRP limit comparisons for the human body model when the vehicle GPS antenna is operated continuously for 30 minutes at an operating frequency of 1.575 GHz are given in detail in Table 14. A cutaway view of the temperature distribution of the three-layer spherical head model after 30 minutes of irradiation is shown in Figure 20.

The peak human body temperature over time is derived in the COMSOL results, as shown in Figure 21.

As can be seen, after 30 minutes of irradiation time under the operating condition of the onboard GPS antenna, the average value of the human-induced electric field, the average SAR of the whole human body, and the temperature rise of the body core of the human model at the three positions inside the electric vehicle do not exceed the

TABLE 11: Performance comparison among proposed and reported antennas.

Ref.	Return loss, S_{11}	Gain	Bandwidth	Axial ratio (dB)
This work	<−20 dB	6.83 dBi	−10 dB, 28 MHz	<3
[30]	—	3.69 dBi	—	3.1
[31]	<−20 dB	3.5 dBi	ARBW3 dB, 50 MHz	1.9
[32]	<−30 dB	5.94 dBi	−10 dB, 39 MHz	2.5
[33]	—	4.12 dBic	ARBW3 dB, 57 MHz	<3
[34]	<−20 dB	4.25 dBi	−10 dB, 14 MHz	<1
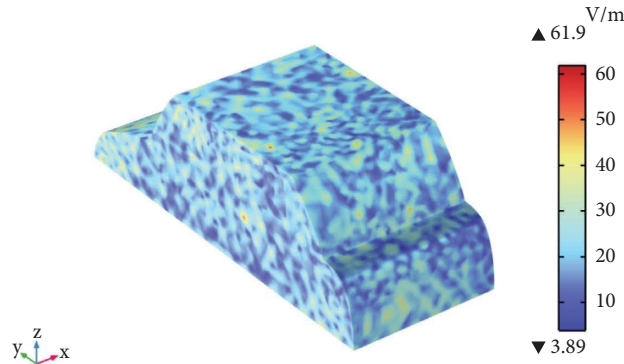
FIGURE 13: Distribution of induced electric field intensity in the car body.

(a)

(b)

(c)

(d)
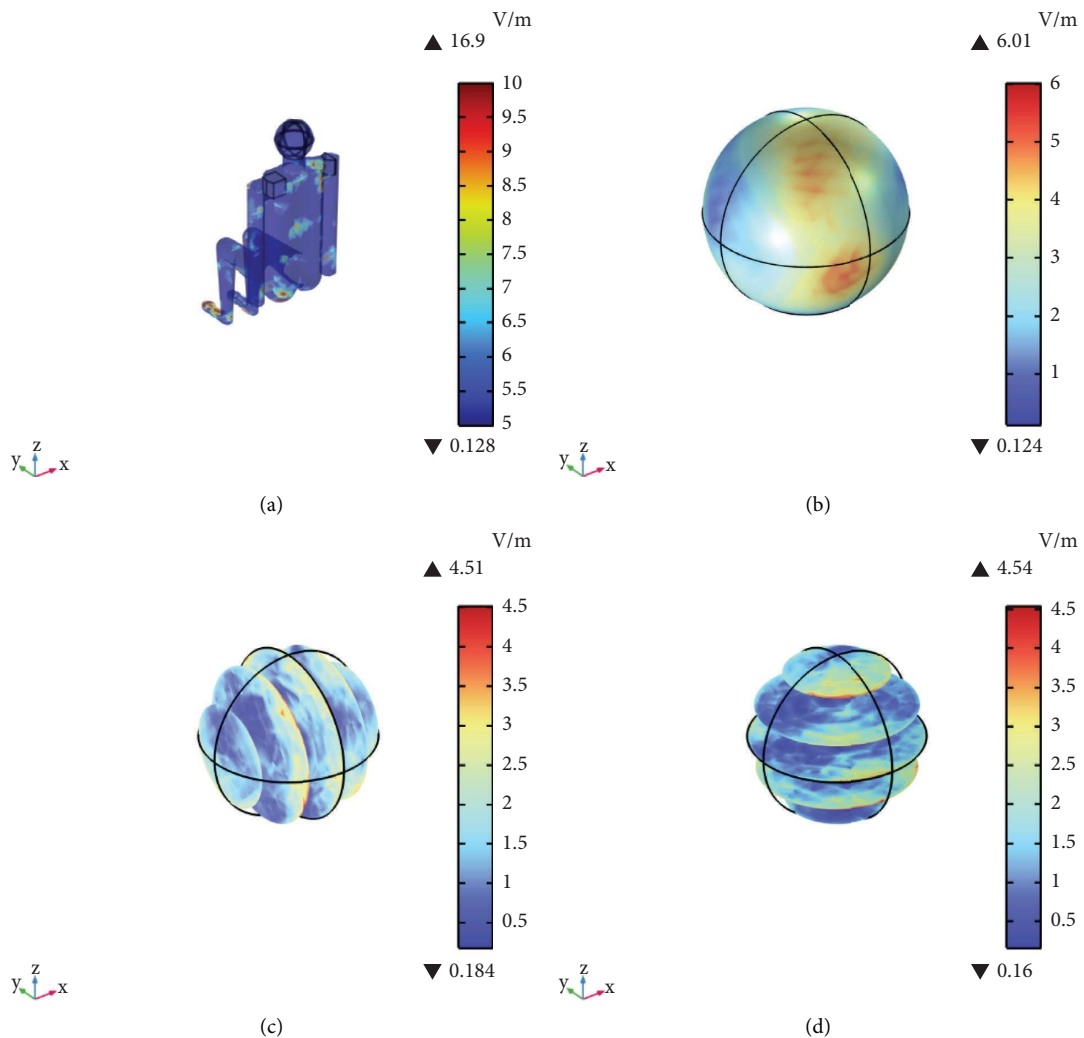
FIGURE 14: Intensity of human-induced electric field in the rear middle seat position (a) for the whole human body, (b) for the head, (c) for the YZ section of head, and (d) for the XY section of head.
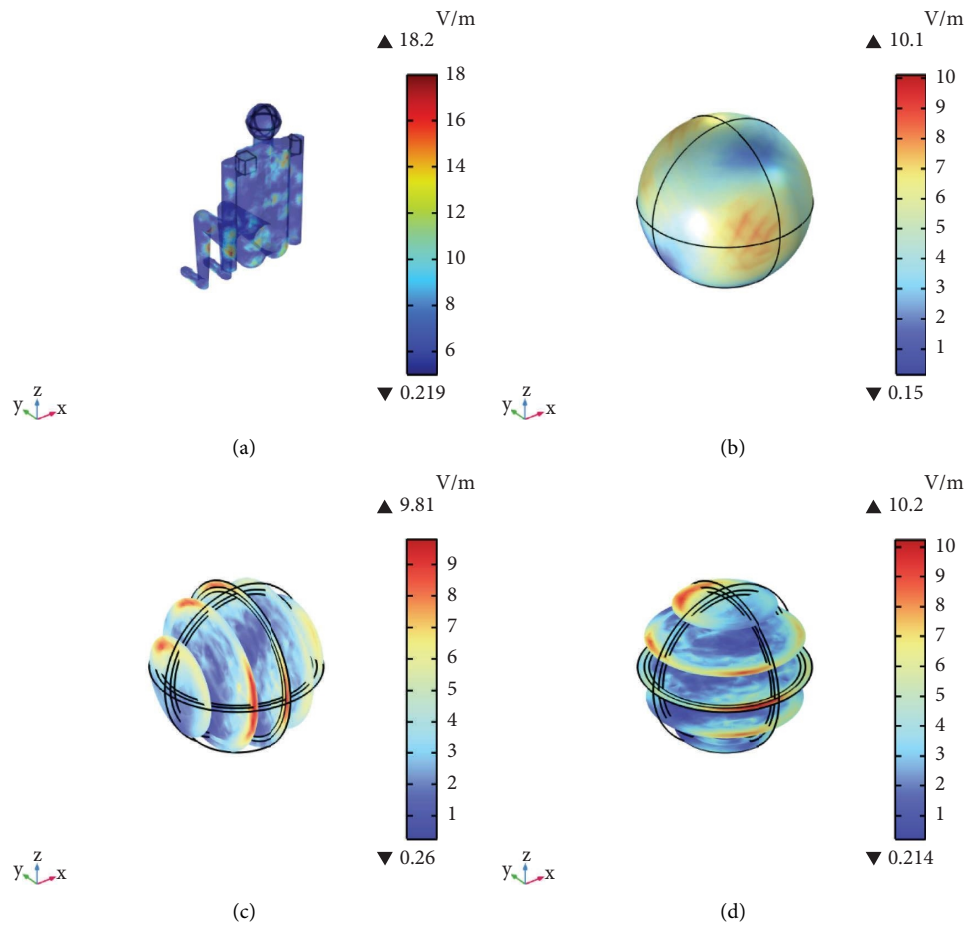
Figure 15: Intensity of human-induced electric field in the rear window seat position (a) for the whole human body, (b) for the head, (c) for the YZ section of head, and (d) for the XY section of head.
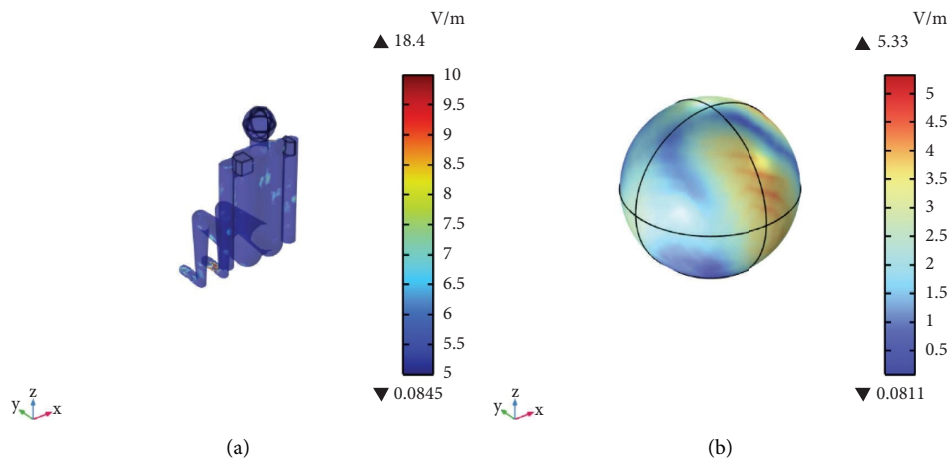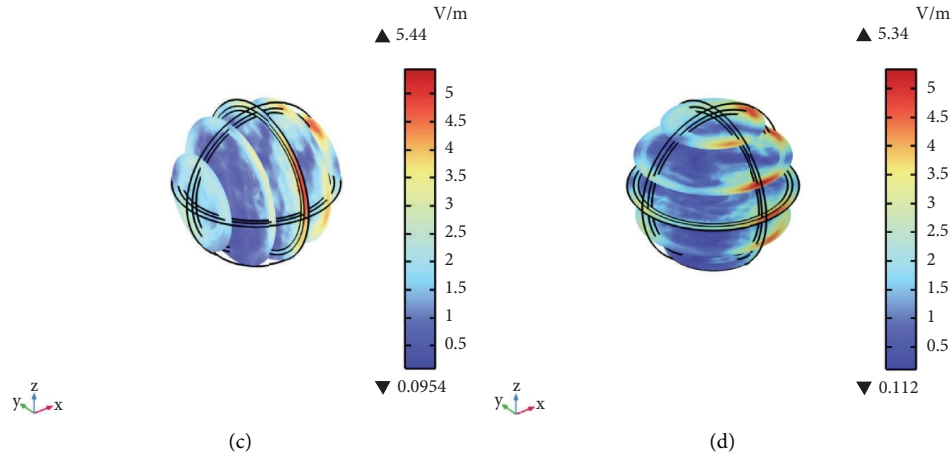

Figure 16: Continued.

(c)

(d)

Figure 16: Intensity of human-induced electric field in the driver's seat position (a) for the whole human body, (b) for the head, (c) for the YZ section of head, and (d) for the XY section of head.

Table 12: Ideal situation, the maximum value, and distribution of human-induced electric field intensity at different positions.

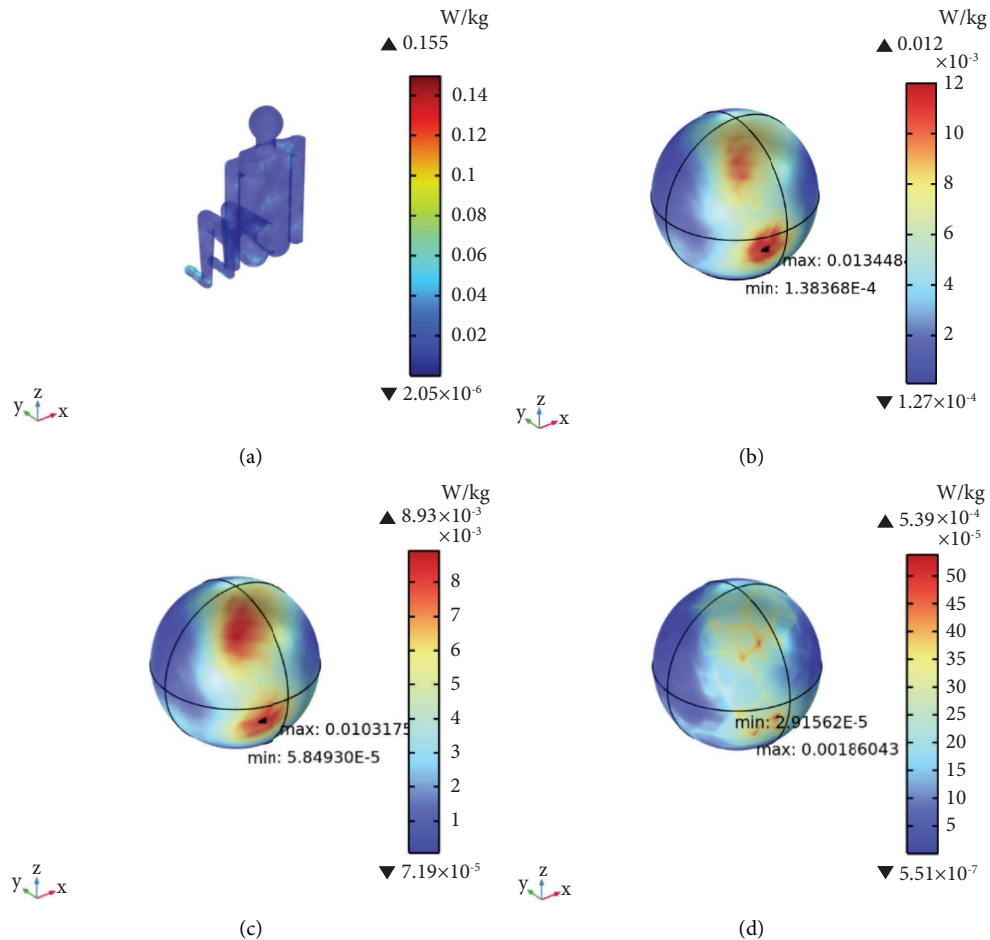| Mannequin position	Rear middle seat position	Rear window seat position	Driver's seat position
Head max (V/m)	6.01	10.1	5.33
Human body maximum (V/m)	16.9	18.2	18.4
Human body maximum appearance site	Bottom of the back	Right hip	Right side of the foot

(a)

(b)
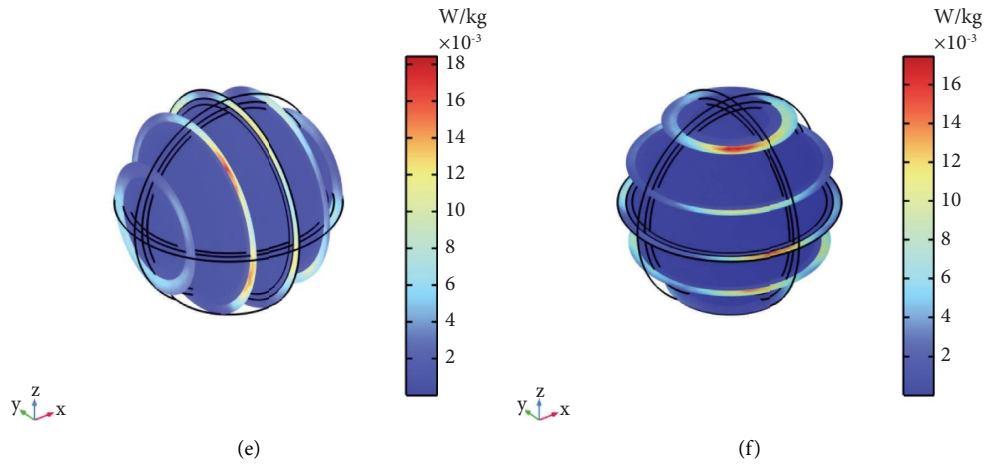

(c)

(d)

Figure 17: Continued.

(e)

(f)

FIGURE 17: Specific absorption rate of the human body in the middle rear seat position (a) for the whole human body, (b) for the scalp layer, (c) for the skull layer, (d) for the cerebrum layer, (e) for the YZ section of head, and (f) for the XY section of head.

(a)

(b)

(c)

(d)

FIGURE 18: Continued.

(e)

(f)

FIGURE 18: Specific absorption rate of the human body in the rear window seat position (a) for the whole human body, (b) for the scalp layer, (c) for the skull layer, (d) for the cerebrum layer, (e) for the YZ section of head, and (f) for the XY section of head.
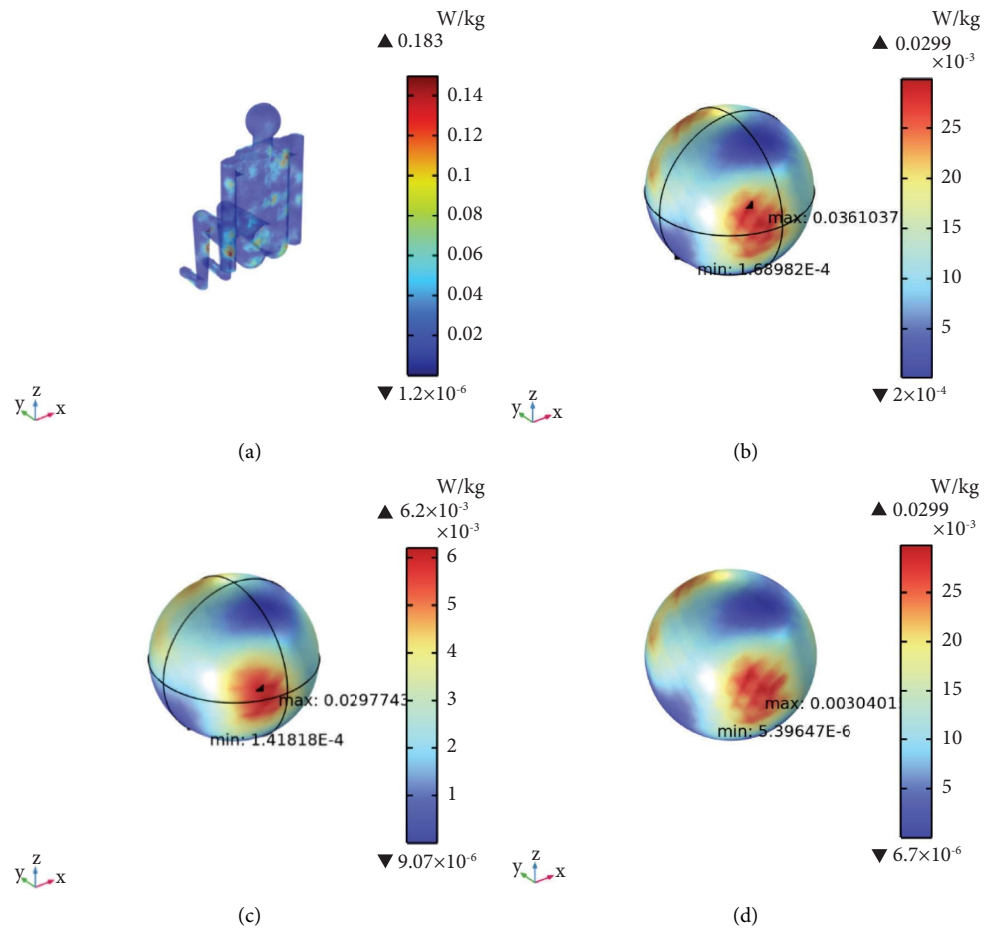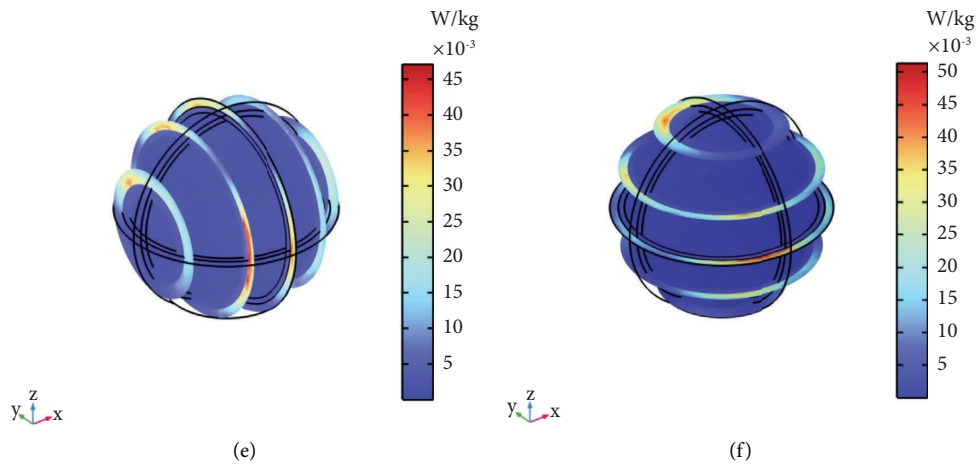

(a)

(b)

(c)

(d)

FIGURE 19: Continued.

(e)   (f)

Figure 19: Specific absorption rate of the human body in the driver's seat position (a) for the whole human body, (b) for the scalp layer, (c) for the skull layer, (d) for the cerebrum layer, (e) for the YZ section of head, and (f) for the XY section of head.
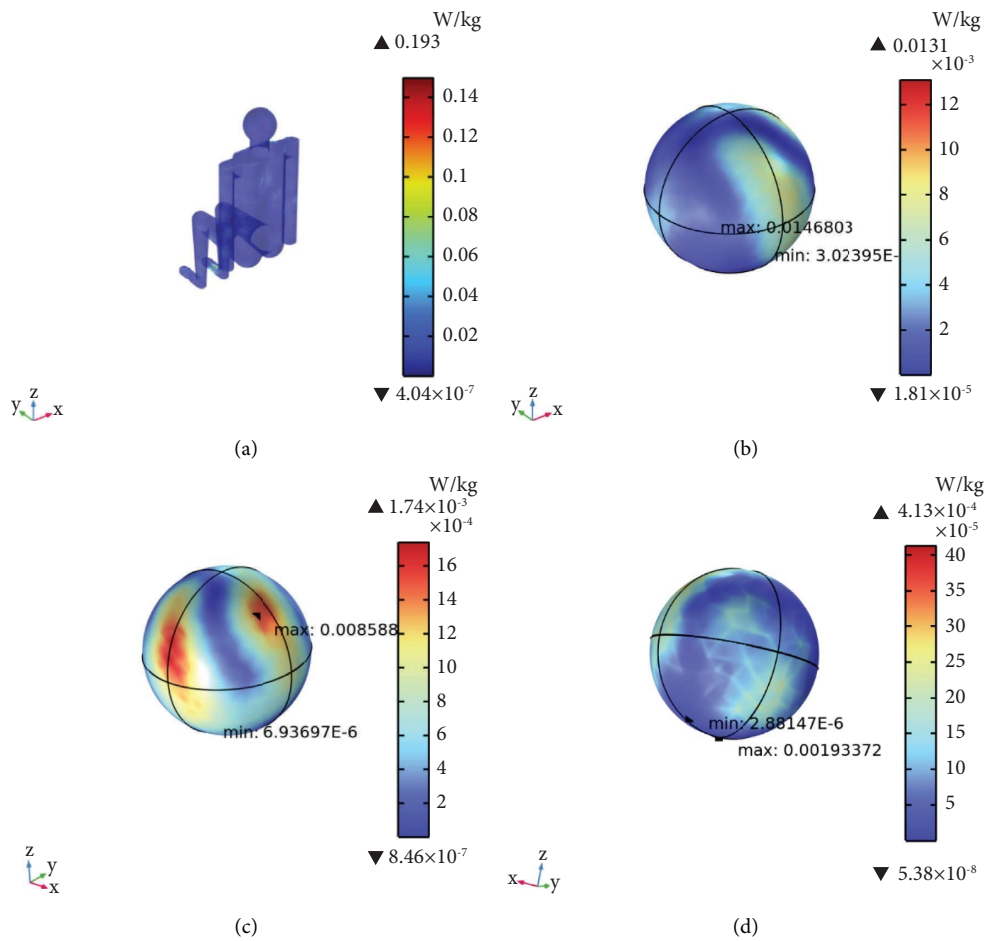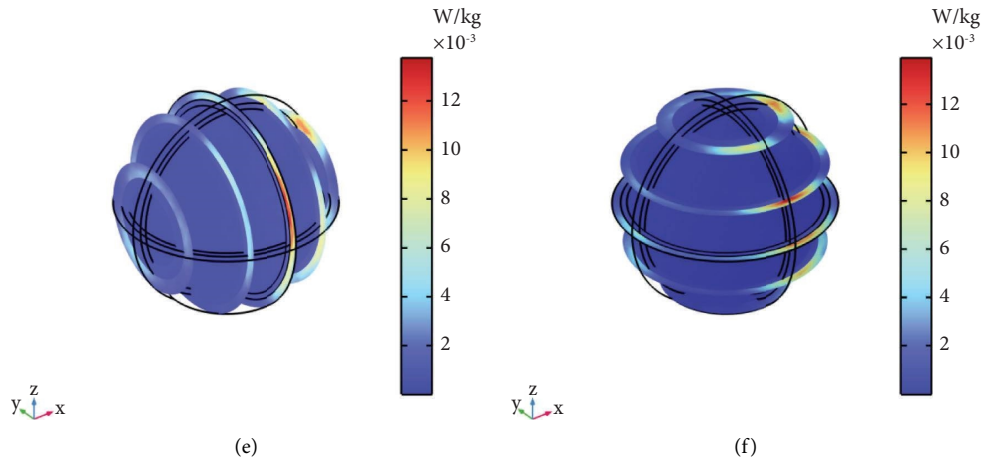
Table 13: Ideal situation and distribution of specific absorption rate of human body at different positions.

Mannequin position	Rear middle seat position	Rear seat window position	Driver's seat position
Human body maximum (W/kg)	0.155	0.183	0.193
Scalp maximum (W/kg)	0.013	0.036	0.015
Skull maximum (W/kg)	0.010	0.030	0.009
Cerebrum maximum (W/kg)	0.002	0.003	0.002

Table 14: Comparison of exposure levels for the whole body over 30 minutes and the ICNIRP guidelines (2020).

Human model	Volume average of the induced electric field E_{inc} (V/m)	Whole-body average SAR (W/kg)	Temperature rise (°C)
The rear middle seat position	1.4678	0.0028	0.0050
The rear window seat position	1.6906	0.0036	0.0600
The driver's seat position	1.4490	0.0017	0.0170
ICNIRP guidelines	54.57	0.0800	1.0000

ICNIRP limits. Therefore, the 30 minute exposure to the human body produced by the car GPS antenna does not produce physiological damage.

From the distribution of temperature field in the head, it can be observed that the scalp layer with the highest electromagnetic power dissipation density has the highest temperature rise, while the skull layer with the lowest power dissipation has the smallest temperature rise. According to Figure 21, the temperature increases rapidly during the early stage of radiation and then gradually slows down after reaching a certain value.

From Table 15, it can be observed that the SAR value and temperature rise caused by GPS antenna radiation on the human body are the lowest compared to medical antennas and mobile phone antennas. This is because GPS antennas typically have lower power levels and are located at a certain distance from the human body. However, due to the prolonged exposure of the body to vehicle-mounted antennas, further research is needed to assess the potential effects of long-term exposure.

4.6. The Impact of Different Vehicle Shell Materials on Human Exposure to Electromagnetic Radiation. Considering that different vehicle body materials can affect the radiation performance of antennas, this study simulated the electromagnetic impact on the human body caused by three typical car shell materials [35–38]. The shell materials were set as PEC, aluminum alloy, and carbon fiber, with their respective dielectric parameters shown in Table 16. Table 17 provides a detailed comparison of the spatial average induced electric field strength, whole-body average SAR value, temperature rise, and ICNIRP limit when the vehicle-mounted GPS antenna operates continuously for 30 minutes at a frequency of 1.575 GHz.
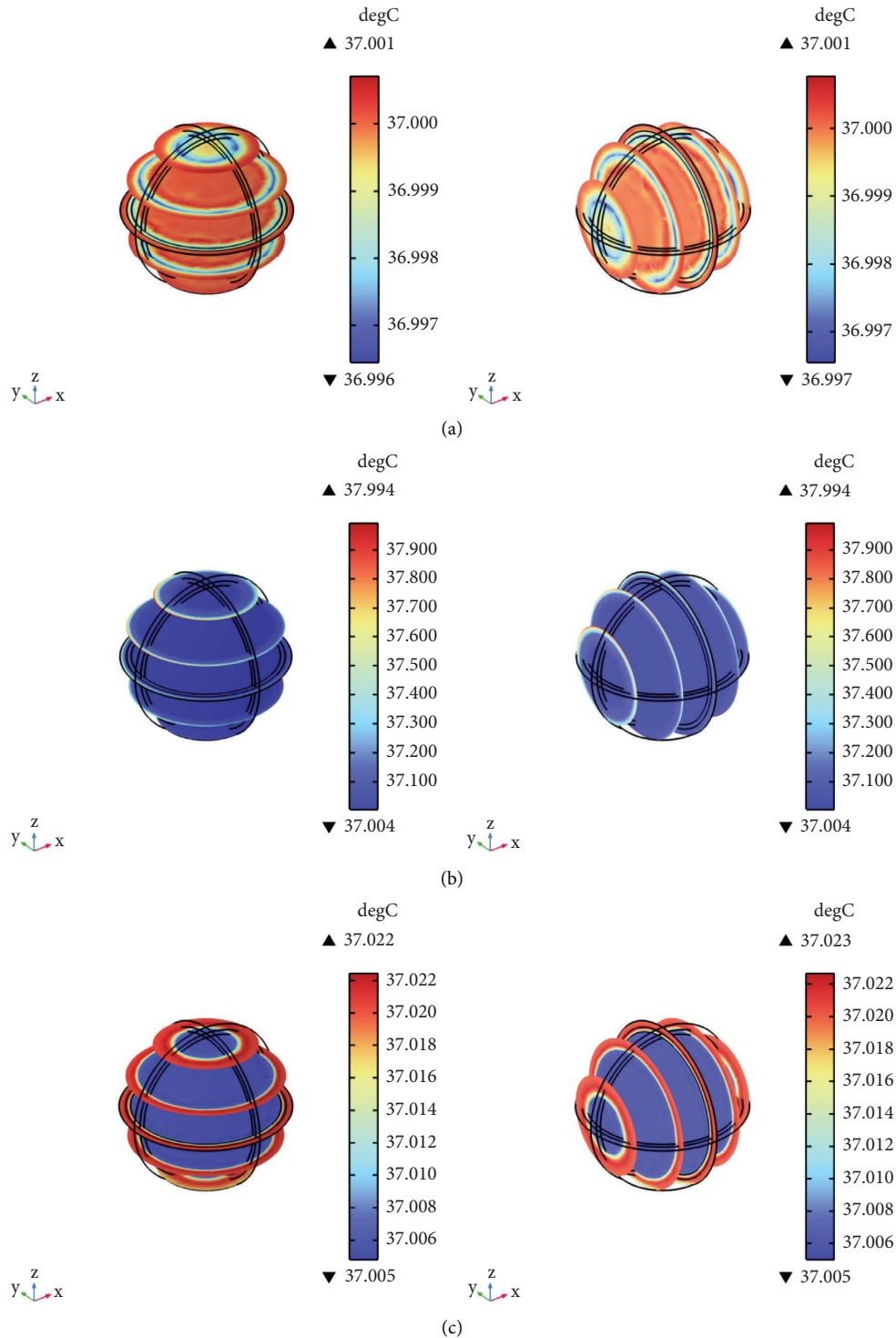
Figure 20: Temperature distribution section of a three-layer spherical head model with 30 minute irradiation. (a) The rear middle seat position. (b) The rear window seat position. (c) The driver's seat position.

The data indicate that the average whole-body exposure level of the human body is significantly below the ICNIRP standard limits. Among the different vehicle shell materials, carbon fiber material results in the highest exposure to electromagnetic radiation. At a frequency of 1.575 GHz, materials with higher relative permittivity and electrical conductivity exhibit better electromagnetic radiation shielding capabilities. Materials with higher relative permittivity cause a slowdown in the propagation of electromagnetic waves within the material, providing better electromagnetic radiation shielding. Materials with high electrical conductivity can effectively absorb and conduct
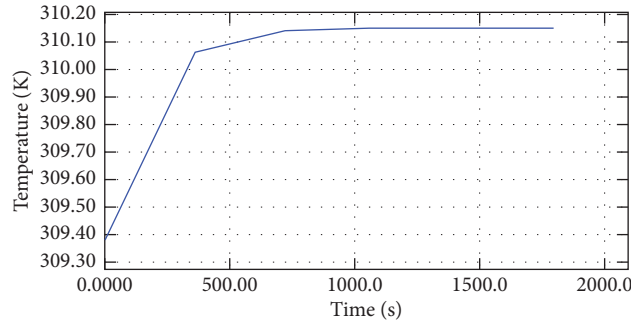
FIGURE 21: Variation of peak human body temperature over time under 30 minutes of electromagnetic radiation.

TABLE 15: Comparison of current work with previous analysis of human exposure to high-frequency electromagnetic fields.

Ref.	Radiation source	Frequency	Averaged SAR maximum value (W/kg)	Temperature rise in 30 minutes
This work	GPS antenna	1.575 GHz	0.0036	0.06
[29]	Rectangular microstrip patch antenna used in the UHF RFID readers	866 MHz	0.012	None
[25]	Dipole antennas in the mobile phone	900 MHz	0.56	None
		1.785 GHz	0.17	0.118

TABLE 16: Vehicle shell materials and their dielectric parameters.

Material	Relative permittivity	Electrical conductivity (S/m)
PEC	∞	∞
Aluminum alloy	2.6	4,032,000
Carbon fiber	2	5000

TABLE 17: Comparison of exposure levels for the whole body over 30 minutes and the ICNIRP guidelines (2020) for different vehicle shell materials.

Material	Volume average of the induced electric field E_{inc} (V/m)	Whole-body average SAR (W/kg)	Temperature rise (°C)
PEC	1.1786	0.0009	0.0501
Aluminum alloy	1.6906	0.0036	0.0600
Carbon fiber	2.5695	0.0051	0.0642
ICNIRP guidelines	54.570	0.0800	1.0000

TABLE 18: The importance of the proposed work.

Comparison factors	Existing methods	Proposed work
Calculating memory and time	Three-layer spherical head simplified model	Reduced
Human position	Three positions	Increased
Physical field	Multiphysics coupling	Comprehensive
Simulation calculation methods	Finite element method (FEM)	High accuracy

electromagnetic radiation energy, reducing its propagation. However, carbon fiber materials exhibit relatively weaker absorption capabilities in the high-frequency range. The data presented in this study can provide some reference for the electromagnetic shielding design of vehicles. However, the optimal choice of shielding materials still depends on specific application requirements and design needs, necessitating practical testing and evaluation to determine the most suitable materials.

5. Conclusion

In this paper, we investigate the electromagnetic exposure generated by the GPS antenna of an electric vehicle. Specifically, we focus on evaluating the induced electric field and the specific absorption rate (SAR) in various tissues of the adult human torso, as well as the three layers of tissues in the scalp, skull, and cerebrum. Our simulations were conducted for three different seating positions: the rear middle seat, the rear window seat, and the driver's seat. To perform these simulations, we employed a multiphysics field approach, utilizing both frequency domain and transient coupling techniques in the COMSOL software.

The purpose is to comprehensively analyze the potential harm caused by the electromagnetic field generated by the GPS antenna. We can also see that the electromagnetic field generated by the GPS is unevenly and unconcentratedly distributed everywhere in the EV. The peak value of human-induced electric field is 18.4 V/m, and the peak value of specific absorption rate is 0.193 W/kg. The average maximum value of human-induced electric field in 30 minutes is 1.6906 V/m, which is 3.1% of the ICNIRP limit; the 30 minute average whole-body SAR maximum is 0.0036 W/kg, which is 4.5% of the ICNIRP limit; and the 30 minute maximum body core temperature rise is 0.06°C, which is 6% of the ICNIRP limit.

Based on the literature review, the advantages of this paper compared to previous similar works are summarized in Table 18.

According to the simulations conducted in this study under specific conditions, the radiation levels of the GPS antenna are considered safe and within the limits set by the International Commission on Non-Ionizing Radiation Protection (ICNIRP). However, in real-world situations, the electromagnetic radiation from in-vehicle GPS antennas is subject to various limitations. For instance, from a material perspective, different materials used for the GPS antenna and vehicle shell exhibit different dielectric properties, which can affect the propagation of electromagnetic waves in and around the antenna, thus influencing the intensity and range of electromagnetic radiation. In terms of time, prolonged operation of the GPS antenna can increase the amount of electromagnetic radiation exposure to the human body. Therefore, when designing and using GPS systems, it is important to consider multiple factors for control and limitation to ensure that human exposure remains within safe levels.

The induced electric field strength, specific absorption rate (SAR) value, and temperature rise in the human body resulting from exposure to the EV GPS antenna are influenced by numerous complex factors. These factors include the operating frequency of the antenna, dielectric properties of the tissues, thermal properties, blood irrigation rate, and more. Further research will focus on developing more realistic human body and antenna models to provide detailed explanations regarding the potential safety risks associated with electromagnetic irradiation from the EV GPS antenna. Ongoing investigations and research into the effects of EV GPS antenna radiation will enhance our understanding of potential risks and help ensure that electromagnetic exposure remains within acceptable limits to protect human health.

Data Availability

All data are available from the corresponding author upon request.

Conflicts of Interest

The authors declare that they have no conflicts of interest.

Acknowledgments

References

[1] Y. X. Guo and D. C. H. Tan, "Wideband single-feed circularly polarized patch antenna with conical radiation pattern," *IEEE Antennas and Wireless Propagation Letters*, vol. 8, pp. 924–926, 2009.

[2] J. Huang, "Circularly polarized conical patterns from circular microstrip antennas," *IEEE Transactions on Antennas and Propagation*, vol. 32, no. 9, pp. 991–994, 1984.

[3] P. Moreno-Torres Concha, P. Velez, M. Lafoz, and J. R Arribas, "Passenger exposure to magnetic fields due to the batteries of an electric vehicle," *IEEE Transactions on Vehicular Technology*, vol. 65, no. 6, pp. 4564–4571, 2016.

[4] H. Tsukahara and M. Hirano, "Numerical analysis of electromagnetic fields around vehicles," in *Proceedings of the IEEE International Symposium on Electromagnetic Compatibility*, pp. 567–571, Washington, DC, USA, August 1990.

[5] Y. Shiraki, K. Sugahara, S. Tanabe, K. Nakamoto, and T. Watanabe, "Electromagnetic field distribution inside an automobile vehicle," in *Proceedings of the 2003 IEEE Symposium on Electromagnetic Compatibility. symposium Record (Cat. No. 03CH37446)*, vol. 2, pp. 730–734, Boston, MA, USA, August 2003.

[6] A. Vassilev, A. Ferber, C. Wehrmann, O. Pinaud, M. Schilling, and A. R. Ruddle, "Magnetic field exposure assessment in electric vehicles," *IEEE Transactions on Electromagnetic Compatibility*, vol. 57, no. 1, pp. 35–43, 2015.

[7] A. Arduino, O. Bottauscio, M. Chiampi et al., "Accuracy assessment of numerical dosimetry for the evaluation of human exposure to electric vehicle inductive charging systems," *IEEE Transactions on Electromagnetic Compatibility*, vol. 62, no. 5, pp. 1939–1950, 2020.

[8] D. Gombarska, M. Smetana, and L. Janousek, "High-frequency electromagnetic field measurement inside personal vehicle within urban environment," in *Proceedings of the*

2019 12th International Conference on Measurement, pp. 223–226, Smolenice, Slovakia, August 2019.

[9] I. A. Shah and H. Yoo, "Assessing human exposure with medical implants to electromagnetic fields from a wireless power transmission system in an electric vehicle," *IEEE Transactions on Electromagnetic Compatibility*, vol. 62, no. 2, pp. 338–345, 2020.

[10] M. O. U. WenTing and L. U. Mai, "Dosimetry simulation research on electromagnetic exposure of wireless charging electric vehicle to human central nervous system," in *Proceedings of the 2021 IEEE 16th Conference on Industrial Electronics and Applications (ICIEA)*, pp. 609–614, IEEE, Chengdu, China, August 2021.

[11] V. De Santis, L. Giaccone, and F. Freschi, "Chassis influence on the exposure assessment of a compact EV during WPT recharging operations," *Magnetochemistry*, vol. 7, no. 2, p. 25, 2021.

[12] P. J. Dimbylow, "FDTD calculations of the SAR for a dipole closely coupled to the head at 900 MHz and 1.9 GHz," *Physics in Medicine and Biology*, vol. 38, no. 3, pp. 361–368, 1993.

[13] J. Yu, X. Ma, Q. Wang, Y. Li, X. Li, and Y. Zheng, "The simulation and research on electromagnetic character and coupling degree of vehicle whip antennas," in *Proceedings of the 2007 International Symposium on Microwave, Antenna, Propagation and EMC Technologies for Wireless Communications*, pp. 1371–1374, Hangzhou, China, August 2007.

[14] A. Hirata and T. Ida, "Analysis of electromagnetic environment in a CAD-based vehicle with a human body for far-field incidence," *IEEE Antennas and Wireless Propagation Letters*, vol. 7, pp. 625–628, 2008.

[15] T. Wessapan, S. Srisawatdhisukul, and P. Rattanadecho, "Specific absorption rate and temperature distributions in human head subjected to mobile phone radiation at different frequencies," *International Journal of Heat and Mass Transfer*, vol. 55, no. 1-3, pp. 347–359, 2012.

[16] A. Kumar and R. S. Imaculate, "Hybrid half-mode SIW cavity-backed diplex antenna for on-body transceiver applications," *Applied Physics A*, vol. 127, pp. 1–7, 2021.

[17] M. Edimo, K. Mahdjoubi, A. Sharaiha, and C. Terret, "Simple circuit model for coax-fed stacked rectangular microstrip patch antenna," *IEE Proceedings- Microwaves, Antennas and Propagation*, vol. 145, no. 3, pp. 268–272, 1998.

[18] J. H. Lu, C. L. Tang, and K. L. Wong, "Single-feed slotted equilateral-triangular microstrip antenna for circular polarization," *IEEE Transactions on Antennas and Propagation*, vol. 47, no. 7, pp. 1174–1178, 1999.

[19] Y. T. Lo, B. Engst, and R. Q. Lee, "Technical memorandum: simple design formulas for circularly polarised microstrip antennas," *IEE Proceedings H Microwaves, Antennas and Propagation*, vol. 135, no. 3, pp. 213–215, 1988.

[20] S. Rush and D. A. Driscoll, "Current distribution in the brain from surface electrodes," *Anesthesia and Analgesia*, vol. 47, no. 6, pp. 717–723, 1968.

[21] S. Rush and D. A. Driscoll, "EEG electrode sensitivity-an application of reciprocity," *IEEE Transactions on Biomedical Engineering*, vol. 16, no. 1, pp. 15–22, 1969.

[22] W. D. Hurt, "Multiterm Debye dispersion relations for permittivity of muscle," *IEEE Transactions on Biomedical Engineering*, no. 1, pp. 60–64, 1985.

[23] S. Gabriel, R. W. Lau, and C. Gabriel, "The dielectric properties of biological tissues: II. Measurements in the frequency range 10 Hz to 20 GHz," *Physics in Medicine and Biology*, vol. 41, no. 11, pp. 2251–2269, 1996.

[24] M. Lu and S. Ueno, "Comparison of the induced fields using different coil configurations during deep transcranial magnetic stimulation," *PLoS One*, vol. 12, no. 6, Article ID 178422, 2017.

[25] P. Bielli, G. Richiardi, P. Bertotto, and A. Schiavoni, "SAR generated by commercial cellular phones-phone modeling, head modeling, and measurements," *IEEE Transactions on Microwave Theory and Techniques*, vol. 48, no. 11, pp. 2064–2071, 2000.

[26] R. J. Spiegel, "A review of numerical models for predicting the energy deposition and resultant thermal response of humans exposed to electromagnetic fields," *IEEE Transactions on Microwave Theory and Techniques*, vol. 32, no. 8, pp. 730–746, 1984.

[27] H. H. Pennes, "Analysis of tissue and arterial blood temperatures in the resting human forearm. 1948," *Journal of Applied Physiology*, vol. 85, no. 1, pp. 5–34, 1998.

[28] International Commission on Non-Ionizing Radiation Protection Icnirp, "Guidelines for limiting exposure to electromagnetic fields (100 kHz to 300 GHz)," *Health Physics*, vol. 118, no. 5, pp. 483–524, 2020.

[29] P. Zradziński, J. Karpowicz, K. Gryz, G. Owczarek, and V. Ramos, "Modelling and evaluation of the absorption of the 866 MHz electromagnetic field in humans exposed near to fixed I-RFID readers used in medical RTLS or to monitor PPE," *Sensors*, vol. 21, no. 12, p. 4251, 2021.

[30] K. Yegin, "On-vehicle GPS antenna measurements," *IEEE Antennas and Wireless Propagation Letters*, vol. 6, pp. 488–491, 2007.

[31] M. Chen and C. C. Chen, "A compact dual-band GPS antenna design," *IEEE Antennas and Wireless Propagation Letters*, vol. 12, pp. 245–248, 2013.

[32] S. Mishra, S. Das, S. S. Pattnaik, S. Kumar, and B. K. Kanaujia, "Low-profile circularly polarized planar antenna for GPS L1, L2, and L5 bands," *Microwave and Optical Technology Letters*, vol. 62, no. 2, pp. 806–815, 2020.

[33] C. Sun, H. Zheng, and Y. Liu, "Analysis and design of a low-cost dual-band compact circularly polarized antenna for GPS application," *IEEE Transactions on Antennas and Propagation*, vol. 64, no. 1, pp. 365–370, 2016.

[34] S. Gupta and G. Mumcu, "Dual-band miniature coupled double loop GPS antenna loaded with lumped capacitors and inductive pins," *IEEE Transactions on Antennas and Propagation*, vol. 61, no. 6, pp. 2904–2910, 2013.

[35] M. Benini, M. Parazzini, M. Bonato et al., "Road user exposure from ITS-5.9 GHz vehicular connectivity," *Sensors*, vol. 22, no. 18, p. 6986, 2022.

[36] Q. Wang, W. Li, J. Kang, and Y. Wang, "Electromagnetic safety evaluation and protection methods for a wireless charging system in an electric vehicle," *IEEE Transactions on Electromagnetic Compatibility*, vol. 61, no. 6, pp. 1913–1925, 2019.

[37] G. Tognola, M. Benini, M. Bonato, S. Gallucci, and M. Parazzini, "Assessment of the variability of human exposure to radiofrequency electromagnetic fields arising from 5.9 GHz vehicular communication in urban environments," *Sensors*, vol. 23, no. 15, p. 6802, 2023.

[38] G. Tognola, B. Masini, S. Gallucci et al., "Numerical assessment of RF human exposure in smart mobility communications," *IEEE Journal of Electromagnetics, RF and Microwaves in Medicine and Biology*, vol. 5, no. 2, pp. 100–107, 2021.